

**Properties and DEFC Tests of Nafion - Functionalized Titanate Nanotubes  
Composite Membranes Prepared by Melt - Extrusion**

B. R. Matos<sup>a</sup>, C. A. Goulart<sup>a</sup>, B. Tosco<sup>b</sup>, J. S. da Silva<sup>a</sup>, R. A. Isidoro<sup>a</sup>, E. I. Santiago<sup>a</sup>,  
M. Linardi<sup>a</sup>, U. Schade<sup>c</sup>, L. Puskar<sup>c</sup>, F. C. Fonseca<sup>a</sup>, A. C. Tavares<sup>d</sup>

<sup>a</sup> Instituto de Pesquisas Energéticas e Nucleares, IPEN-CNEN/SP, São Paulo 05508000, Brazil.

<sup>b</sup> Universidade Federal do ABC, UFABC. Santo André, SP, 09219170, Brazil.

<sup>c</sup> Methoden der Materialentwicklung, Helmholtz-Zentrum für Materialien und Energie GmbH, Berlin, 12489 Germany.

<sup>d</sup> Institut National de la Recherche Scientifique - Énergie, Matériaux et Télécommunications (INRS-EMT), 1650 Boulevard Lionel-Boulet, Varennes, Québec, Canada, J3X 1S2.

\*corresponding author: B. R. Matos (email: [brmatos@usp.br](mailto:brmatos@usp.br))

**Keywords:** melt-extrusion; sulfonic acid functionalization; nanotubes; composites; ionomer.

## **Abstract**

Nafion based composites are promising materials to improve the performance of direct ethanol fuel cells. In this work, composite membranes of Nafion and titanate nanotubes functionalized with sulfonic acid groups were prepared by melt-extrusion and tested in a direct ethanol fuel cell. Far and mid infrared spectroscopies evidenced the formation of ionic bridges between the sulfonic acid groups of both functionalized nanoparticles and the ionomer. Small angle X-ray scattering measurements revealed that the melt - extrusion method leads to an uniform distribution of the inorganic phase in the ionomer matrix. Such structural analysis indicated that the improved the proton conduction properties of the composites, even with the addition of a high concentration of functionalized nanoparticles, are an outcome of the synergistic ionic network due to the hybrid organic/inorganic proton conducting phases. However, an improvement of the fuel cell performance is observed for 2.5 wt% of functionalized titanate nanotubes, which is a result of the lower ethanol crossover and the plasticizing effect of the aliphatic segments of the organic moieties grafted at the surface of the titanate nanoparticles.

## Introduction

Composite electrolyte membranes based on the incorporation of an inorganic phase into ionomer matrices often show enhanced properties, such as high mechanical resistance and low permeability to solvents compared to the pristine ionomer membranes [1,2,3,4,5]. These properties are of paramount importance in direct alcohol fuel cells (DAFC), in which high mechanical resistance is required for reducing the plasticization of the solid electrolyte by the liquid fuel, and the low fuel crossover is necessary to minimize the depolarization of the cell [1,2]. However, one of the main drawbacks associated with composite membranes is the low proton conductivity of the electrolyte, since the nanoparticles are usually poor proton conductors. Another challenge, specific to DAFCs, is the poor proton conduction in alcoholic media [4].

The most commonly used nanoparticles are based on metal oxide materials such as SiO<sub>2</sub>, TiO<sub>2</sub>, ZrO<sub>2</sub>, etc. [5,6,7]. Such particles possess high specific surface area and high hydrophilicity, but are characterized by a lower proton conductivity ( $\sigma \sim 10^{-4} \text{ Scm}^{-1}$ ) compared to Nafion ( $\sigma \sim 10^{-1} \text{ Scm}^{-1}$ ) [5]. In alternative, some efforts have been dedicated to the development of Nafion composite membranes containing proton conducting inorganic phases such as titanate nanotubes (H<sub>2</sub>Ti<sub>3</sub>O<sub>7</sub>.nH<sub>2</sub>O), zirconium phosphate (Zr(HPO)<sub>4</sub>), and functionalized metal oxide nanoparticles [8,9,10,11]. It was reported that surface functionalized titanate nanotubes display a proton conductivity of  $\sigma \sim 10^{-2} \text{ Scm}^{-1}$ , which is attractive for fuel cell applications.

Another important strategy is the addition of fiber-like nanoparticles into polymer matrices, which are known to enhance the water retention properties and the ion conductivity [4]. In addition, nanoparticles with a high aspect ratio increase substantially the mechanical properties of the polymer composites [9,12]. Furthermore, fiber-like mineral nanoparticles, in analogy with the titanate nanotubes, were shown to

boost the proton conductivity by increasing the connectivity within the inorganic phase into the composite membranes [13].

The distribution of the nanoparticles in the ionomer matrix affects directly the direct ethanol fuel cell (DEFC) performance using the composites. For example, Nafion-Titanate nanotubes have been prepared by casting and hydrothermal methodologies [9]. The former produces composite membranes with a poor distribution of the inorganic phase, whereas in the latter a fine dispersion of the nanotubes in the ionomer matrix is obtained. When uniformly dispersed in the matrix, the inorganic particles form an extended interface with the nanometric ionic domains of Nafion, leading to a higher connectivity of the ionic domains and creating new conduction pathways for proton migration [14]. In addition, a substantial enhancement of the mechanical properties and reduction of the alcohol crossover of the Nafion-Titanate prepared by hydrothermal method was observed compared to commercial Nafion membranes and to the Nafion-titanate prepared by casting.

Nonetheless, the casting methodology has the advantage of allowing the use of nanoparticles with distinct morphologies and functionalization prior to the fabrication of the composite solid electrolyte [9,14]. A preparation methodology that has been poorly explored for the preparation of composite ionomer membranes for fuel cells is the extrusion technique [15,16,17,18]. Twin melt-extrusion method consists of compounding mixtures of organic-inorganic phases in a broad range of compositions prior to passing matter through a orifice of well-defined shape. Twin extrusion offers a higher degree of dispersion of the nanoparticles within the polymer matrix, since both organic and inorganic phases are mixed at the melting point of the polymer by the extrusion screws [14,15]. The extrusion technique has attracted increasing importance for the preparation of electrolyte films for DAFC as being a cheaper production method

of composite materials compared to traditional solution-casting [15]. Furthermore, the use of extrusion brings several beneficial aspects for the DAFC performance, for example: *i*) it also allows the use particles of different morphologies and surface chemistries; *ii*) extruded materials display higher degree of crystallinity, which may increase the mechanical robustness of the film, and more importantly, lower methanol crossover [15-18].

Herein, composite membranes based on Nafion and titanate nanotubes functionalized with sulfonic acid groups were prepared by melt-extrusion. The composites were characterized by far and mid infrared spectroscopy (FIR and MIR), small angle X-ray scattering (SAXS), impedance spectroscopy (IS) and were tested in direct ethanol fuel cell. The new Nafion-titanate composites display a high degree dispersion of the inorganic phase within the ionomer matrix, and the functionalization of the titanate nanotubes resulted in a strong interaction between the nanoparticles and Nafion's ionic aggregates. Such features promoted an increase of the proton conductivity with increasing inorganic phase content and an improvement of the DEFC performance.

## **Experimental**

### *Functionalization of the titanate nanotubes (TNTf)*

The titanate nanotubes were prepared by an alkaline hydrothermal process by autoclaving a NaOH solution ( $10 \text{ mol L}^{-1}$ ) containing titania anatase nanoparticles (Degussa) at  $110 \text{ }^\circ\text{C}$  for 24h, as described elsewhere [21]. The functionalization of the titanate nanotubes was performed by dispersing the titanate nanotubes in anhydrous toluene containing 3-mercaptopropyltrimetoxysilane (3-MPTMS / 95% solution, Alfa Aesar) under continuous stirring. The grafting reaction was carried out under stirring at

60 °C for 6 h in a balloon bottle, and the MPTMS/TNT ratio varied from 10 to 60 wt%. The samples were filtered and washed with toluene twice and dried at 50°C in vacuum for 2h. Details on the preparation and characterization of the titanate nanotubes can be found in previous publications [9,10,11].

The titanate nanotubes grafted with 3-MPTMS were used to prepare the Nafion composites, since the extrusion process is more difficult when the materials are in the ionic form because ionic crosslinks exist in the molten state [22]. Therefore, the oxidation of the silane moieties grafted at the titanate nanotubes surface to sulfonic acid groups ( $\text{RSH} \rightarrow \text{RSO}_3\text{H}$ ) was performed after the extrusion process along with the standard cleaning and activation of the composite membrane.

#### *Preparation of the Nafion – Functionalized titanate nanotubes composite membranes*

The Nafion - functionalized titanate nanotubes (TNTf) composites were prepared by extrusion using a XPlore Conic Twin-Screw Micro-Compounder (~ 5 mL of capacity). The extruded composite cords were fabricated under co-rotation at 300 rpm and  $T = 230$  °C, using mixtures of Nafion precursor (sulfonyl fluoride form /  $1100 \text{ gmol}^{-1}$ , Ion Power<sup>®</sup>) and different concentrations of TNTf ranging from 0 to 15 wt% (ex.: N-TNTf-0, N-TNTf-2.5, N-TNTf-5, N-TNTf-10 and N-TNTf-15). The segments of the extruded cords were hot-pressed at  $T = 200$  °C (polymer only) and at  $T = 230$  °C (composites) and a pressure of  $200 \text{ kgfcm}^{-2}$  for 2 min. Right after the hot-pressing, the films underwent quenching by immersing them for 2 min in liquid  $\text{N}_2$  to suppress the samples' recrystallization. The presence of a high degree of crystallinity in Nafion was reported to reduce the degree of ionic conversion in the sample bulk with respect to the surface [23].

At this stage, both the polymer and the grafted titanate nanotubes must undergo the conversion of their functional groups into the sulfonic acid form. First, the SO<sub>2</sub>F groups of Nafion were converted into SO<sub>3</sub>Na. This reaction was carried out by placing the Nafion and the composite films in a water/DMSO/NaOH solution (50/35/15 vol%) for 6 h at 80 °C. The membranes were cleaned 3 times with deionized water for 1 h at 80 °C. Next, the mercapto groups of the titanate nanotubes were oxidized to SO<sub>3</sub>H groups by placing the composite membranes in a H<sub>2</sub>O<sub>2</sub> (3 vol%) solution for 1 h at 80 °C. The acidification of Nafion composites was performed in three steps: two treatments in HCl solution (0.1 molL<sup>-1</sup>) and one last one at H<sub>2</sub>SO<sub>4</sub> (0.5 molL<sup>-1</sup>) at 80 °C for 1 h. All these steps were intermediated by washing with deionized water at 80 °C for 1 h to remove the excess of chemicals.

#### *Physicochemical characterization of the functionalized nanotubes and composite membranes*

The morphology of the titanate nanotubes was studied by field-emission scanning electron microscopy (FE-SEM, JEOL model JSM-6701F). Transmission electron microscopy (TEM) images of the titanate nanotubes were recorded using a JEOL-2100F instrument with 200 kV of applied voltage.

The CHNS analysis, also known as dynamic flash combustion method, was carried out on the functionalized samples in order to quantify the amount of grafted silane from the percentage of S. CHNS elemental analyses of the functionalized nanotubes were performed in the Elemental Analysis Laboratory of the University of Montreal, using an analyzer EAS1108, Fisons Instruments S.p.A. Specifically, the sample (~ 2 mg) is weighed and put in a tin capsule, and introduced in to a quartz tube reactor under a flow of He enriched with O<sub>2</sub>. The sample and the tin capsule react with

oxygen at 1700-1800 °C, and are broken into their elemental components, N<sub>2</sub>, CO<sub>2</sub>, H<sub>2</sub>O and SO<sub>2</sub>. The gas composition is analyzed by a thermal conductivity detector, and a signal proportional to the amount of each element in the sample is generated. The elemental peaks are compared to a known standard and the elemental wt% quantified. The accuracy of the results is ± 5% for each element.

N<sub>2</sub> sorption isotherms of the functionalized titanate nanotubes were measured at -196 °C down to relative pressure  $P/P_0$   $5 \times 10^{-7}$  with Quantachrome Instrument Autosorb. The samples were weighed and placed on the analysis port. Before the sorption measurement, each sample was heated at 60 °C for 2h under vacuum. The specific surface area was obtained by the BET method, while the micropore and the mesopores volumes were determined by applying the *t*-plot de Boer and the BJH methods, respectively. The sorption data were analysed using Autosorb Software from Quantachrome Instrument.

The equivalent weight (*EW*) of the composite membranes was determined by acid-base titration using the relation  $EW = m/Mv$ ; where *m* is the dry mass of the composite recorded after acidification treatment; *M* is the solution molarity; and *v* is the titrated volume. The membranes in the H<sup>+</sup> form were placed in a 1 M NaCl solution for 30 min and the proton concentration back titrated with a 0.01 M NaOH solution, standardized with potassium biphthalate. The water uptake (*WU*) was obtained as the ratio between the mass of the absorbed water by the mass of dry polymer.

Mid infrared (MIR) Fourier Transform (FT) spectroscopy measurements were performed with a Nicolet 6700 spectrometer in the attenuated total reflectance (ATR) mode using a ZnSe crystal. Each spectrum is an average of a total of 96 scans with a spectral resolution of 4 cm<sup>-1</sup> in the 4000 to 600 cm<sup>-1</sup> range at room *T* (25 °C) and *RH* (40%). For these measurements, the composite samples were previously dried in a

vacuum oven for 1 h at room  $T$  and immediately placed at the spectrometer to avoid extensive absorption of water from the environment.

Far infrared (FIR) and MIR FT spectra were also measured at the IRIS beamline at the electron storage ring BESSY II of Helmholtz Zentrum Berlin [24]. The measurements for both FIR and MIR were done in transmission mode in vacuum ( $< 0.1$  mbar) in the sample compartment of a Bruker Vertex 70/v spectrometer. FIR spectra in spectral region between 600 and 30  $\text{cm}^{-1}$  were measured with 2  $\text{cm}^{-1}$  resolution using infrared synchrotron radiation as a source together with a liquid helium cooled silicon bolometer and a silicon beamsplitter. For these measurements 128 scans were co-added. For the MIR transmission measurements the internal globar source was employed together with a DLaTGS detector and a KBr beamsplitter. The spectra were taken at 4  $\text{cm}^{-1}$  resolution and 32 scans were co-added. For both the spectral regions investigated, references were taken through the empty channel inside the spectrometer sample compartment under vacuum. The data acquisition started when no more changes in the water related features were observed spectroscopically.

SAXS experiments were carried out using synchrotron radiation at the SAXS beamline of the Brazilian National Synchrotron Light Laboratory (LNLS). The experiments were conducted with an incident wavelength  $\lambda = 1.488 \text{ \AA}$  in the range of the scattering vector  $q \sim 0.02\text{--}0.35 \text{ \AA}^{-1}$  ( $q = 4\pi \sin \theta/\lambda$ , with  $2\theta$  being the scattering angle). Scattering patterns were collected with MarCCD detector and the intensity curves corrected for parasitic scattering, integral intensity, and sample absorption.

Impedance spectroscopy (IS) data were collected in an especially designed air-tight sample holder able to measure the proton conductivity in the range  $T = 30 - 200 \text{ }^\circ\text{C}$  with  $RH = 100\%$  [19]. A Solartron 1260 frequency response analyzer was used for IS measurements in 4 mHz to 3 MHz frequency ( $f$ ) range with 100 mV *ac* amplitude. The

resistance of the samples was obtained from the intercept of the impedance semicircle at high frequencies ( $f \sim 10^6$  Hz) with the real axis of the complex plane [25]. The measurements were performed in triplicates, and the associate experimental error is 10%.

Differential scanning calorimetry (DSC) was performed on dry Nafion with DSC Q200 – TA instruments under nitrogen flow in two successive heating scans from -50 to 250 °C at a heating rate of 20 °C min<sup>-1</sup> under nitrogen flow. A fast cooling step (50 °C min<sup>-1</sup>) was used between the heating steps. The thermal event observed in the first heating associated with the order-disorder transition of the sulfonic groups is absent in the second heating (not shown), following the typical behavior observed for Nafion [31].

#### *Direct Ethanol Fuel Cell tests*

Extruded Nafion and the composite membranes were evaluated in 5 cm<sup>2</sup> single fuel cells. MEAs were fabricated by hot pressing both electrodes to the fabricated membranes at 125°C and 1000 kgf cm<sup>-2</sup> for 2 min. The anode catalyst layer was composed of 1.0 mg cm<sup>-2</sup> PtSn/C (Pt:Sn of 75:25 Etek) and 30 wt% of dry Nafion (Dupont). The cathode catalyst layer contained 1.0 mg cm<sup>-2</sup> Pt/C (20%, Etek) and 30 wt% Nafion. The thicknesses of the hydrated membranes were ~ 160 μm. The single cell was fed at the anode with 1.0 mol L<sup>-1</sup> ethanol solution and 5.0 mL min<sup>-1</sup> flux at 1 atm, and at the cathode with pure oxygen at 3 atm absolute pressure. Fuel cell and oxygen humidifier temperatures were varied from 80 °C to 110 °C and polarization curves were obtained in duplicate experiments with estimated error of ~10% between 80 °C and 110 °C. For each measuring temperature, after temperature stabilization the system was

conditioned by draining electrical current at a fixed voltage of 0.7 V for 2 h before data collection in order to reach steady state.

## Results and Discussion

**Figure 1a** shows the SEM images of the titanate nanotubes, and the corresponding high magnification image obtained by TEM is shown in **Fig. 1b**.

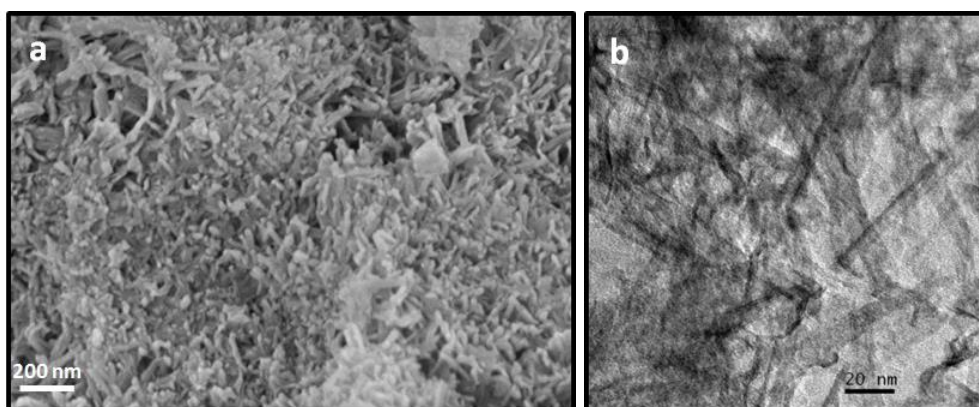


**Figure 1.** SEM (a) and TEM (b) images of the titanate nanotubes in the proton form.

The images of the titanate nanotubes show a distribution of a relatively large volume fraction of nanoparticles with an average diameter of  $\sim 10$  nm and length of  $\sim 100$  nm, in good agreement with reported typical nanotube dimensions [9,21]. The titanate nanotubes consist typically of 3-5 multiple layers tubes with internal and external diameters ranging between 3-5 and 7-10 nm, respectively, and characteristic length of hundreds of nanometers (100-300 nm) [9,21]. **Fig. 1b** evidences the tubular nanostructures with characteristic dimensions compatible to the ones usually reported for titanate nanotubes in the powder form, confirming the exit in the preparation of the inorganic phase.

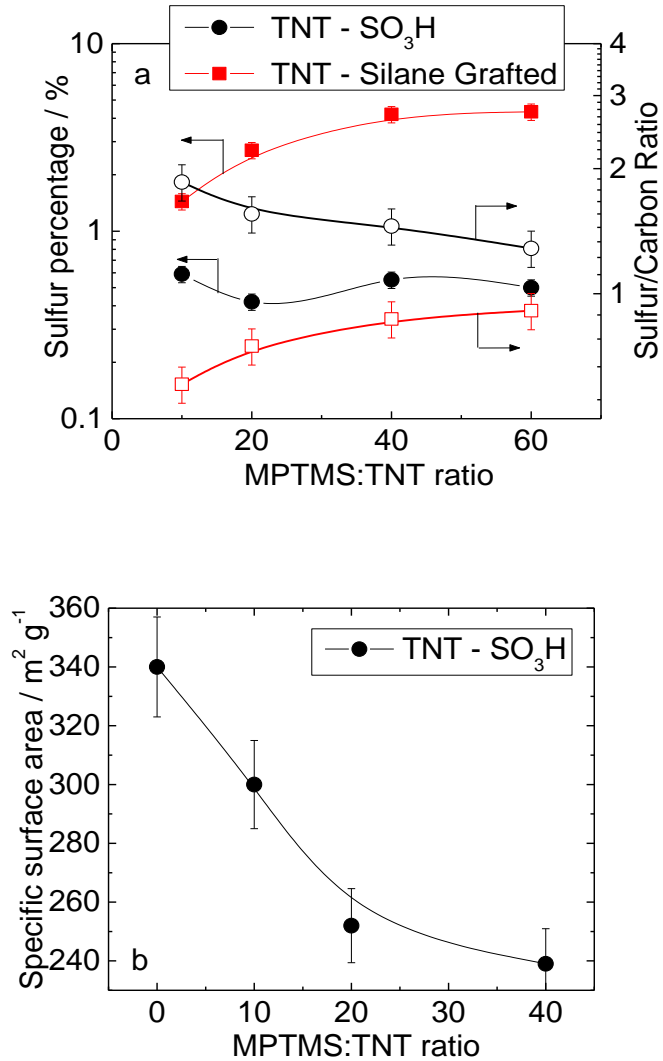


**Figure 2.** (a) Sulfur content of the modified titanate nanotubes (left axis) and sulfur/carbon percentage ratio (right axis) with the 3-MPTMS/TNT ratio, before and after the oxidation of the thiol groups. (b) Specific surface area of the grafted titanate nanotubes with the 3-MPTMS/TNT ratio.

**Fig. 2a** shows the variation of sulfur content in the modified titanate nanotubes with the MPTMS/TNT ratio before and after the oxidation of the thiol groups. Prior to the silane oxidation, the sulfur content on the titanate nanotubes increases with the MPTMS concentration in the grafting solution. A plateau is nevertheless observed for MPTMS/TNT ratio > 40 suggesting that at high silane concentration, a fully coverage

of the surface of the titanate nanotubes takes place [26]. Such hypothesis is confirmed by the ratio S/C which increases with increasing MPTMS/TNT in a similar trend. In contrast, after the conversion of the thiol groups into sulfonic acid groups, the amount of sulfur is fairly constant among all samples. However, the S/C ratio decreases with increasing MPTMS/TNT ratio in the entire range investigated. Such trends indicate that the self-polymerization of the mercapto – precursor competed with the grafting reaction on the surface of the nanotubes, and that the non-grafted MPTMS is washed away during the washing and oxidation steps [3,26].

In **Fig. 2b** it is shown that the specific surface area of the nanotubes decreases from  $340 \text{ m}^2\text{g}^{-1}$  for the non-modified TNT to  $240 \text{ m}^2\text{g}^{-1}$  (40wt%), which is consistent with an increase of the extent of grafting, and possibly a reduced porosity of the grafted nanotube surface [3,26]. Considering both the sulfur content and the specific surface area of the functionalized nanotubes, nanotubes obtained from 40 wt% MPTMS/TNT were chosen for preparing the composite samples.

FTIR spectroscopy was used to investigate the conversion of the Nafion precursor into its ionic form, and of the  $-\text{SH}$  into  $\text{SO}_3\text{H}$  groups in the composite membranes. Representative spectra are shown in **Fig. 3**. The spectrum of Nafions' non-ionic form contains a band at  $1470 \text{ cm}^{-1}$  assigned to the  $\text{SO}_2$  stretching in  $\text{SO}_2\text{F}$  [27]. After the conversion, the typical vibrational bands of Nafion can be observed in the FTIR spectra (**Fig. 3a** and **3b**). The band at  $1060 \text{ cm}^{-1}$  is assigned to the symmetric S-O stretching vibrations from the  $\text{SO}_3^-$  groups. The bands at  $1220$  and  $1150 \text{ cm}^{-1}$  are attributed to the symmetric and asymmetric stretching of  $\text{CF}_2$ , respectively. And the bands at  $980$  and  $960 \text{ cm}^{-1}$  are assigned to the symmetric vibrations from two C-O-C linkages residing in two distinct chemical environments [22,24,28].

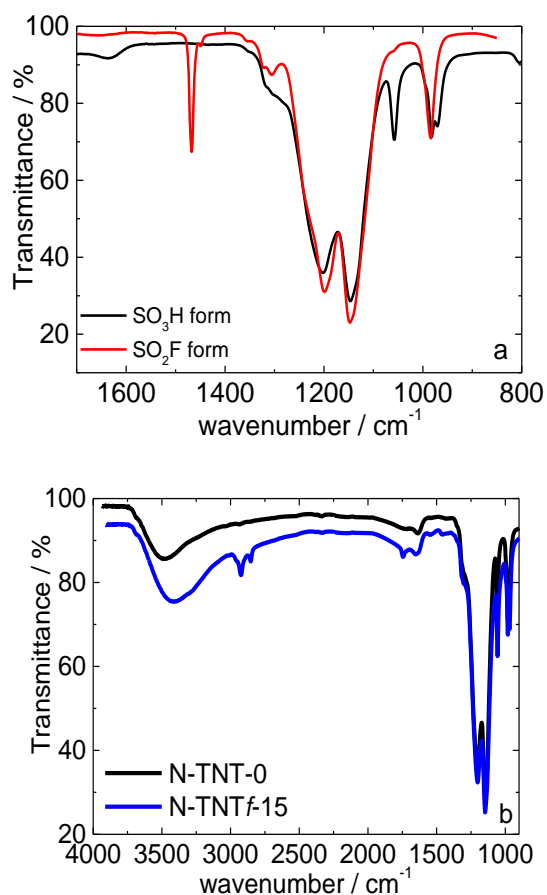


**Figure 3.** FTIR-ATR spectra of (a) Nafion precursor ( $\text{SO}_2\text{F}$  form) and converted into the  $\text{SO}_3\text{H}$  form; and (b) melt extruded Nafion (N-TNT-0) and composite Nafion-titanate nanotubes (N-TNTf-15) membranes.

In **Fig. 3b**, the spectrum of Nafion containing functionalized titanate nanotubes (N-TNTf-15) displays additional peaks at 2918 and 2844  $\text{cm}^{-1}$ , assigned to the grafted C-H moieties in the inorganic phase [29,30]. The transmittance spectrum of N-TNTf-15 displays no noticeable band in the 2550 – 2620  $\text{cm}^{-1}$  range, which is consistent with the conversion of the anchored thiol groups [29,30]. The conversion of the thiol groups originating from the sulfonyl fluoride matrix and from the anchored thiol groups can also be attested by ion exchange capacity measurements. According to these measurements, the functionalization of the titanate nanotubes contributed the ion exchange capacity of the composites, which increased with the content of the inorganic

phase: N-TNTf-2.5 ( $\sim 0.92 \text{ mEqg}^{-1}$ ), N-TNTf-5 ( $\sim 0.95 \text{ mEqg}^{-1}$ ), N-TNTf-10 ( $\sim 1.00 \text{ mEqg}^{-1}$ ), N-TNTf-15 ( $\sim 1.07 \text{ mEqg}^{-1}$ ). These values are very close to the expected value of ion exchange capacity ( $\sim 0.90 \text{ mEqg}^{-1}$ ). The water uptake of the all composites is nearly constant (30 wt%), but is higher than that of the melt-extruded Nafion membrane (NTNTf-0, 24wt%) in excellent agreement with the higher amount of acidic groups in the composites.

Evidence the cation motion of the translational motion of protons along the ionic clusters in Nafion can be given by Far infrared measurements [22,24]. Yet, to first characterize the state of aggregation of the sulfonic acid groups in the functionalized TNTs, Nafion sulfonyl fluoride composites were treated with  $\text{H}_2\text{O}_2$  and  $\text{H}_2\text{SO}_4$  only. As expected, the FIR spectrum of pristine polymer films that underwent such treatment displays only the characteristic bands of the nonionic form [22]. **Figures 4a** and **4b** show in addition the far ( $500 - 20 \text{ cm}^{-1}$ ) and mid infrared spectra ( $4000 - 1250 \text{ cm}^{-1}$ ) respectively, of N-TNTf in the  $\text{SO}_2\text{F}$  form.

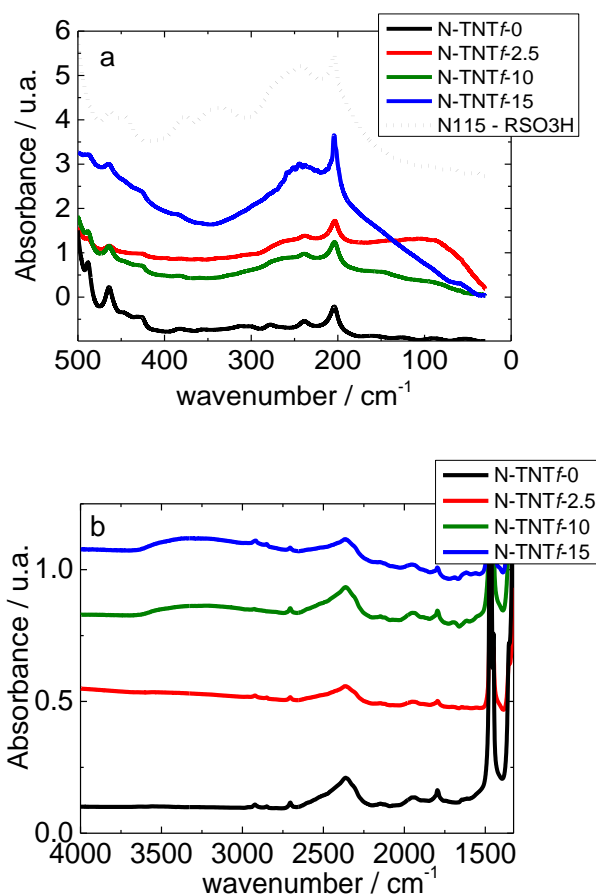


**Figure 4.** (a) Far ( $500 - 20 \text{ cm}^{-1}$ ) and (b) mid ( $4000 - 1300 \text{ cm}^{-1}$ ) infrared spectra recorded under vacuum and in the transmission mode of composite films formed by N-TNTf and Nafion in the  $\text{SO}_2\text{F}$ . The spectra of Nafion in the ionic and non-ionic forms are shown for comparison.

The spectrum of N-TNTf ( $\text{SO}_2\text{F}$ ) differs from that of Nafion- $\text{SO}_2\text{F}$  by the presence of a broad band in the  $350 - 50 \text{ cm}^{-1}$  range, peaking at  $\sim 250 \text{ cm}^{-1}$ . This band is clearly identified in the N-TNTf-15 spectrum, and is attributed to a convolution of bands associated with the cation motion within  $\text{SO}_3\text{H}$  clusters ( $240 \text{ cm}^{-1}$ ) and the typical bands of Ti-O vibrations in titanate nanotubes lattice ( $181$  and  $270 \text{ cm}^{-1}$ ). Nafion's typical  $\text{CF}_2$  rocking band is seen at  $204 \text{ cm}^{-1}$ . The spectrum of Nafion in the proton form also shows three bands at  $\sim 240$ ,  $335$ , and  $375 \text{ cm}^{-1}$  which are assigned to H-bond

stretching involving the hydronium ion in  $\text{RSO}_3\text{H}$  [22,24]. Since the FTIR measurements were performed under vacuum, the water sorption by these samples is negligible, resulting in the absence of the 335 and 375  $\text{cm}^{-1}$  bands (**Fig. 4a**). The band associated with the hydrogen bonding within  $\text{SO}_3\text{H}$  groups (3200  $\text{cm}^{-1}$ ) is present in the spectra of the composites with concentrations of the inorganic phase above  $> 2.5\text{wt}\%$ , **Fig. 4b**. The observed OH stretching band may be due to the hydrogen bonding among titanate nanotube particles and among sulfonic acid groups. It is important to stress that the presence of ionic clusters in the nanoparticles can help improving the connectivity of the conduction pathway for proton transport in the ionomer matrix.

SAXS measurements were performed to evaluate the distribution of the nanoparticles in the Nafion matrix. **Fig. 5a** displays a comparison of the SAXS patterns of the N-TNT composites in the  $\text{SO}_3\text{H}$  form prepared by different methods: casting, sol-gel and extrusion (N-TNTf-2.5). **Fig. 5b** shows the SAXS patterns of N-TNTf composites and of Nafion in the  $\text{SO}_2\text{F}$  form.

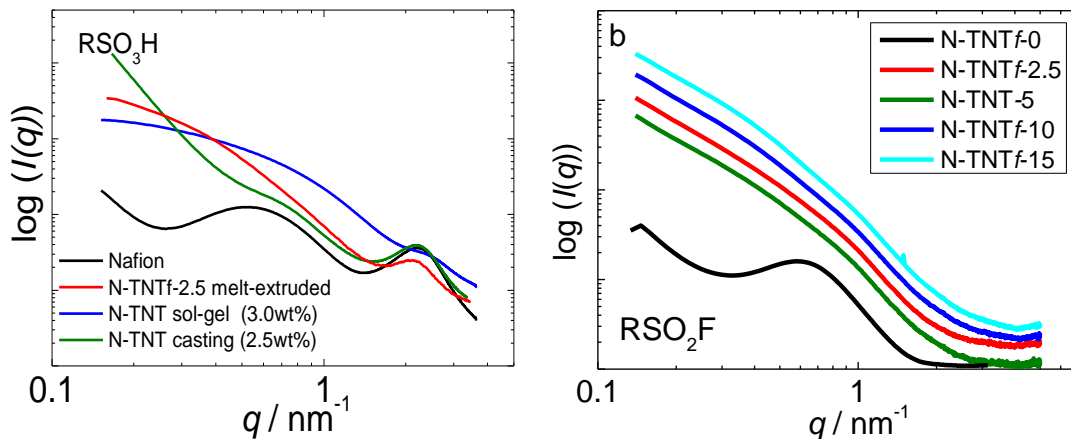


**Figure 5.** Comparison of SAXS patterns from (a) N-TNT composites in the  $\text{SO}_3\text{H}$  form prepared by different methods: casting, sol-gel and extrusion (N-TNTf-2.5); (b) melt - extruded composites in the sulfonyl fluoride form with different amounts of functionalized titanate nanotubes.

As illustrated in the figure, Nafion's SAXS pattern displays the matrix peak at  $q \sim 0.6 \text{ nm}^{-1}$  and the ionomer peak at  $q \sim 2 \text{ nm}^{-1}$  [23]. Instead, the SAXS plots of the composites display only the ionomer peak, because the matrix peak is superposed with the X-ray scattering from the nanoparticles at  $q < 2 \text{ nm}^{-1}$ . The differences between the scattering patterns of the composites at low  $q$  are the result of difference in the distribution of the inorganic phase in the ionomer matrix. The casting method produces composite membranes with a poor distribution of the titanate nanotubes, as indicated by the upturn in scattering intensity at  $q < 0.6 \text{ nm}^{-1}$ , which is mostly due to the correlation length among the nanoparticles, and indicates a higher degree of aggregation of nanoparticles of the composites prepared by casting. On the other hand, the SAXS curves of Nafion-titanate samples prepared by sol-gel and melt-extrusion exhibit scattering patterns forming a plateau for  $q < 0.3 \text{ nm}^{-1}$ , which suggests that such scattering is associated with the shape of the nanoparticles, and an absence of interparticle correlation. This feature indicates a low degree of aggregation among the nanoparticles. Still, the SAXS measurements of the N-TNTf in the nonionic form (**Fig. 5b**) display a linear dependence for  $q < 0.3 \text{ nm}^{-1}$  indicating some agglomeration of nanoparticles. The differences between the SAXS curves at low  $q$  ( $q < 0.3 \text{ nm}^{-1}$ ) for N-TNT in the nonionic and ionic forms (**Figs. 5a** and **b**) may be also due to scattering differences in the ionomer matrix due to ionic conversion [22]. However, compared with the composites prepared by casting, the melt-extruded composites do not exhibit an increase of the particle aggregation with increasing the inorganic phase content, as shown in **Fig. 5b**. Such feature evidences the ability of preparing composites with a wide range of composition displaying a high degree of homogeneity.

**Figure 6** shows the Arrhenius plots for the proton conductivity of Nafion and the N-TNT $f$  composites. The Arrhenius plots were built using the proton conductivity values obtained from the high frequency intercept in the impedance spectra ( $Z'' \rightarrow 0$  at  $f \sim 10^6$  Hz) of fully hydrated membranes. It was previously shown that at such frequency range, the motion of protons corresponds to forward-backward fluctuations of high mobility protons across a nanometer length-scale ( $\sim 10^{-1}$  to  $10^1$  nm) in hydrated domains of Nafion [25].

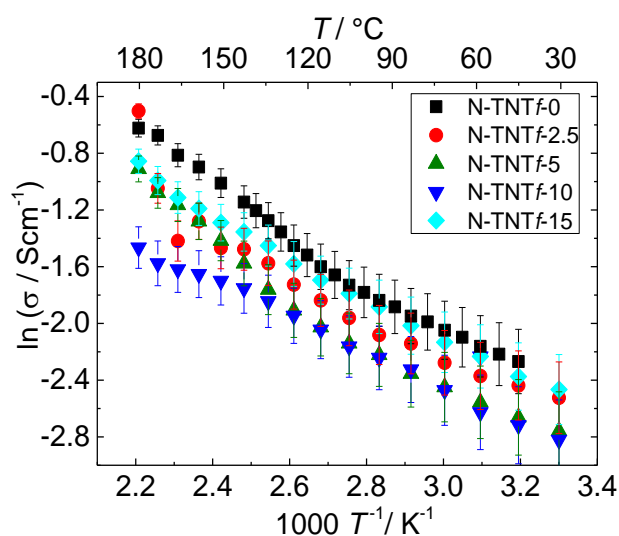


**Figure 6.** Arrhenius plots for the proton conductivity of Nafion and the N-TNT $f$  composites. Impedance spectroscopy measurements were done at 100% RH.

The proton conductivity of the composites is lower than the one observed for melt - extruded Nafion. The lower conductivity of the composites with respect to the pristine Nafion is probably due to the lower proton conductivity of functionalized titanate nanotubes ( $10^{-2}$  Scm $^{-1}$ ) [21]. Still, an important aspect of the N-TNT $f$  composites, and not found in the ones prepared by the other methods [9,10,11], is the higher proton conductivity of N-TNT $f$ -15 compared to that of the composites with lower fractions of TNT $f$ . In addition, the drop of conductivity is much smaller in the

N-TNTf composites compared to the those usually observed for composite membranes prepared with titania or silica nanoparticles [5,9,29].

Nafion displays an upturn of the proton conductivity for  $T > 90$  °C, which is due to a crossover from the Arrhenius-like to the Vogel-Tamman-Fulcher (VTF) temperature dependence of the proton conductivity [19]. Such upturn is not observed in the composite samples. In fact, the proton conductivity for the composites at  $T > 90$  °C does not follow the VTF behavior which has been related to the modulation of the proton transport by thermally activated correlated motion of the main and side chains. The different conductivity – temperature behavior of the composite membranes is an evidence that the hydrocarbon grafted chains are contributing to the proton transport in the sample. Such feature is in good agreement with the FTIR data and may be the reason for the higher proton conductivity for the composites with high concentration of nanoparticles (N-TNTf-15). Specifically, the addition of grafted titanate nanotubes improves the phase separation into the ionic and nonionic domains, increasing the mean free path for proton migration. Moreover, according to the Vogel-Tamman-Fulcher empirical law, the nonlinear increase of the proton conductivity with increasing  $T$  is associated with a temperature dependent reduction of the viscosity of the medium for glass-like materials [32]. In polymer systems, such phenomenon is associated with a cooperative motion between the proton transport and the mobility of the main and side chains. The higher flexibility of the polymer chains due to the plasticizing effect of the grafted moieties may contribute positively to the proton conductivity of the composite membranes.

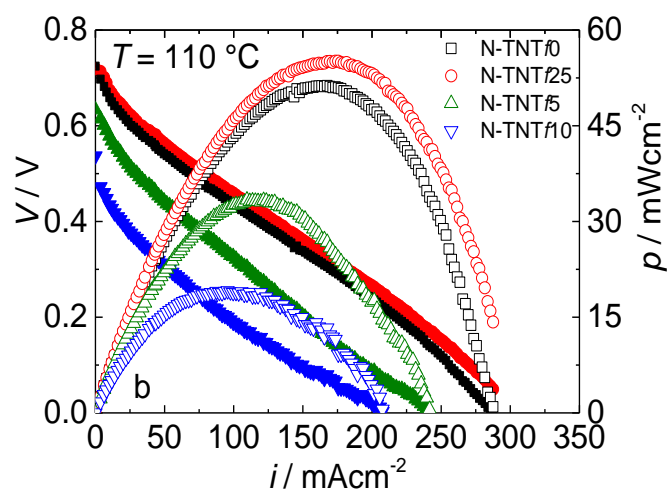


**Figure 7.** DEFC polarization curves and power densities recorded obtained at 110 °C with the composite electrolytes. The fuel cell is fed with 1M ethanol solution at 5 mL min<sup>-1</sup> rate (1atm) at the anode and with O<sub>2</sub> at 3 atm at the cathode.

**Figure 7** shows that the DEFC performance of the N-TNT $f$ -2.5 composite is higher than that of Nafion. The addition of a small amount of functionalized nanoparticles into Nafion, resulting in composite membranes with higher water sorption capacity and higher proton conductivity compared to composite membranes prepared from non-functionalized ones, is indeed a promising strategy to improve the fuel cell efficiency. However, the performances of composites with higher content of nanoparticles are significantly lower. In particular, the DEFCs show a lower open circuit voltage, which is usually associated with a high fuel crossover across the membrane. Besides, no substantial changes of the slope in the ohmic region of the polarization curve are observed, in good agreement with the proton conductivity measurements.

In fact, the N-TNT $f$  composites exhibit higher macroscopic flexibility than the composites prepared with non-functionalized nanoparticles. As a result, composites with high nanoparticles content could not be tested at  $T$  above 130 °C due to the

formation of pinholes, pointing for a low thermomechanical property of these films. In order to evaluate the thermal behavior of the composite membranes, DSC measurements were carried out and the results are shown in **Fig. 8**.

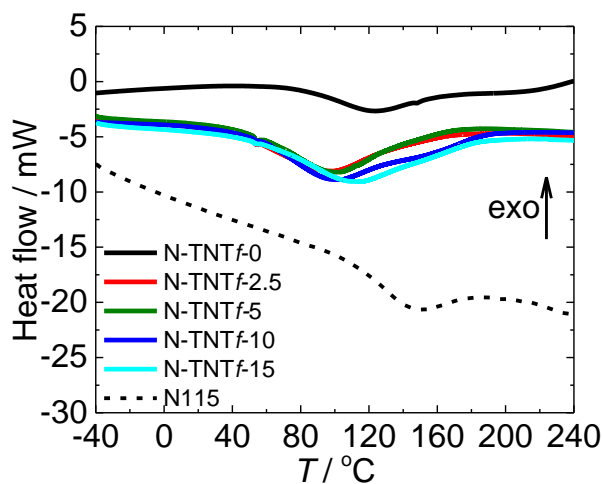


**Figure 8.** DSC scans of the melt-extruded N-TNTf composite membranes.

The DSC scan of N115 displays an endothermic minimum centered at 145 °C, which is characterized as the relaxation of the hydrogen bonding among sulfonic acid groups, usually termed as  $\alpha$ -transition [33]. The DSC scans of the composite membranes exhibit a marked shift of such minimum from 145 to 97 °C for N-TNTf-2.5 indicating that the addition of TNT functionalized with sulfonic groups contributed to the weakening of the electrostatic interactions among sulfonic groups into the composite. However, with increasing of the fraction of TNTf from 2.5 to 15%, the endothermic minima shifted from 97 to 112 °C and a second endothermic peak appears around 150 °C for TNTf  $\geq$  10wt%. These results suggest that higher loadings of the TNTf may bring beneficial effects to the thermomechanical properties of the Nafion-TNTf composites. It has been previously reported that the neutralization of Nafion with alkylammonium counterions with different lengths of the hydrophobic moieties promoted a plasticization of the hydrophobic parts of Nafion chains and reduced

significantly ( $\sim 50$  °C) the  $\alpha$ -transition temperature [28,31]. The DSC results raise a question on the effect of the length of the C-H moieties of the TNTf on the mechanical and electrical properties of functionalized composites. Possibly, the self-polymerization of the silane precursor results in longer hydrocarbon chains that will favor interactions between the functionalized nanoparticles and the hydrophobic domains of Nafion. Since the ethanol molecules display affinity for both hydrophilic and hydrophobic phases of Nafion, the existence of higher fractions of flexible hydrophobic phase and higher water uptake into Nafion-Titanate composites may contribute to the increase of the permeability to ethanol in the membranes. Such investigation is a topic of further communication and is out of the scope of this work.

## **Conclusions**

The use of melt-extrusion technique allowed producing composite membranes of Nafion-titanate nanotubes aggregating several important synergistic features that are known to maximize the proton conductivity. The extrusion method used permitted preparing Nafion with addition of high surface specific area and acid sulfonic functionalized titanate nanotubes with a higher degree of distribution of the inorganic phase into the ionomer matrix, even for high-load composites as revealed by SAXS. Moreover, FIR measurements allowed discerning that the additional ionic groups contained in the inorganic phase are interacting with the ionic domains of Nafion. The intimate supramolecular interactions of the organic and inorganic phases contributed to increase the composite water content and, more importantly, to increase the proton conductivity with increasing inorganic phase. The DEFC performance was improved for

composites with 2.5wt% titanate nanotubes content, indicating that melt-extruded composites are promising materials for DEFC electrolytes.

### **Acknowledgements**

Laboratório Nacional de Luz Síncrotron (projects n° 17722 e n° 18801). A.C. Tavares kindly acknowledges the funding support from NSERC (Canada, program Discovery Grant). Authors acknowledge the support of CNEN-IPEN, FAPESP [2014/09087-4], the RCGI Research Centre for Gas Innovation, FAPESP [2014/50279-4], and the CINE Center for Innovation on New Energies - Shell (ANP) / FAPESP [2017/11937-4]. FCF, EIS, ML, RAI and CAG are fellows of CNPq.

### **References**

- [1] X. Li, E. P. L. Roberts, S. M. Holmes, Evaluation of composite membranes for direct methanol fuel cells, *J. Power Sources*, 154 (2006) 115-123.
- [2] Song, S.; Tsiakaras, P. Recent Progress in Direct Ethanol Proton Exchange Membrane Fuel Cells (DE-PEMFCs). *Appl. Catalysis B: Environ.* 63 (2006) 187-193.
- [3] B. Mecheri, V. Felice, Z. Zhang, A. D'Epifanio, S. Licoccia, A. C. Tavares, DSC and DVS investigation of water mobility in Nafion/Zeolite composite membranes for fuel cell Applications, *J. Phys. Chem. C* 116 (2012) 20820.
- [4] Z. Zhang, F. Désilets, V. Felice, B. Mecheri, S. Licoccia, A. C. Tavares, On the proton conductivity of Nafion–Faujasite composite membranes for low temperature direct methanol fuel cells, *J. Power Sources*, 196 (2011) 9176-9187.
- [5] B. R. Matos, R. A. Isidoro, E. I. Santiago, F. C. Fonseca, Performance enhancement of direct ethanol fuel cell using Nafion composites with high volume fraction of titania, *J. Power Sources*, 268 (2014) 706-711.
- [6] D. Cozzi, C. de Bonis, A. D'Epifanio, B. Mecheri, A. C. Tavares, S. Licoccia Organically functionalized titanium oxide/Nafion composite proton exchange membranes for fuel cells applications, *J. Power Sources* 248 (2014) 1127-1132.
- [7] B. Mecheri, V. Felice, A. D'Epifanio, A. C. Tavares, S. Licoccia, Composite Polymer Electrolytes for Fuel Cell Applications: Filler-Induced Effect on Water Sorption and Transport Properties, *Chem. Phys. Chem.* 14 (2013),3814-3821.

- [8] Truffier-Boutry, D.; De Geyer, A.; Guetaz, L.; Diat, O.; Gebel, G. Structural Study of Zirconium Phosphate–Nafion Hybrid Membranes for High-Temperature Proton Exchange Membrane Fuel Cell Applications, *Macromolecules* 40 (2007) 8259.
- [9] B. R. Matos, R. A. Isidoro, E. I. Santiago, M. Linardi, A. S. Ferlauto, A. C. Tavares, F. C. Fonseca, In Situ Fabrication of Nafion–Titanate Hybrid Electrolytes for High-Temperature Direct Ethanol Fuel Cell, *J. Phys. Chem. C*, 117 (2013) 16863-16870.
- [10] B. R. Matos, E. I. Santiago, J. F. Q. Rey, A. S. Ferlauto, E. Traversa, M. Linardi, F. C. Fonseca, Nafion-based composite electrolytes for proton exchange membrane fuel cells operating above 120 C with titania nanoparticles and nanotubes as fillers, *J. Power Sources*, 196 (2011) 1061-1068.
- [11] B. R. Matos, E. I. Santiago, F. C. Fonseca, M. Linardi, V. Lavayen, R. G. Lacerda, L. O. Ladeira, A. S. Ferlauto, Nafion–titanate nanotube composite membranes for PEMFC operating at high temperature, *J. Electrochem. Soc.*, 154 (2007) B1358-B1361.
- [12] F. Xu, S. Mu, M. Pan, Decoration of Carbon Nanotube with SiO<sub>2</sub> Nanoparticles to Improve Polyelectrolyte Membrane Performance, *J. Nanosci. Nanotechnol.* 11 (2011) 10896–10899,
- [13] F. Xu, S. Mu, M. Pan, Mineral nanofibre reinforced composite polymer electrolyte membranes with enhanced water retention capability in PEM fuel cells, *J. M. Sci.* 377 (2011) 134– 140.
- [14] Alberti, G.; Casciola, M. Composite Membranes for Medium-Temperature PEM Fuel Cells. *Annu. Rev. Mater. Res.* 33 (2003) 29-154.
- [15] Y. Treekamol, M. Schieda, L. Robitaille, S. M. MacKinnon, A. Mokrini, Z. Shi, S. Holdcroft, K. Schulte, S. P. Nunes, Nafion®/ODF-silica composite membranes for medium temperature proton exchange membrane fuel cells, *J. Power Sources* 246 (2014) 950-959.
- [16] A. Mokrini, N. Raymond, K. Theberge, L. Robitaille, C. Del Rio, M. C. Ojeda, P. G. Escibano, J. L. Acosta, Properties of melt-extruded vs. solution-cast proton exchange membranes based on PFSA nanocomposites, *ECS Transactions* 33 (2010) 855-865.
- [17] A. Mokrini, A. Siu, L. Robitaille, L. Gonzalez, F. Sanchez, Investigation of advanced hybrid PEM based on sulfonyl fluoride PFSA and grafted inorganic nanoparticles, *ECS Transactions* 33 (2010) 823-838.
- [18] A. Mokrini, M. A. Huneault, Z. Shi, Z. Xie, S. Holdcroft, Non-fluorinated proton-exchange membranes based on melt extruded SEBS/HDPE blends, *J. Mem. Sci.* 325 (2008) 749-757.

- [19] B. R. Matos, C. A. Goulart, E. I. Santiago, R. Muccillo, F. C. Fonseca, Proton conductivity of perfluorosulfonate ionomers at high temperature and high relative humidity, *Appl. Phys. Lett.*, 104 (2014) 091904.
- [20] Mark, J.E. in *Hybrid Organic-Inorganic Composites*, (Eds: Mark, J.E.; Y-C Lee, C.; Bianconi, P.A.), ACS Symposium Series, Vol. 585. American Chemical Society. Washington, DC. 1995. Ch 1.
- [21] Bavykin, D. V.; Friedrich, J. M.; Walsh, F. C. Protonated Titanates and TiO<sub>2</sub> Nanostructured Materials: Synthesis, Properties, and Applications. *Adv. Mater* 18 (2006) 2807-2824.
- [22] B. R. Matos, R. Politano, J. F. Q. Rey, D. Hermida-Merino, U. Schade, L. Puskar, F. C. Fonseca, Interplay of  $\alpha/\beta$ -Relaxation Dynamics and the Shape of Ionomer Building Blocks, *Scientific Reports*, 8 (2018) 13441.
- [23] M.-H. Kim, C. J. Glinka, S. A. Grot, W. G. Grot, SANS Study of the Effects of Water Vapor Sorption on the Nanoscale Structure of Perfluorinated Sulfonic Acid (NAFION) Membranes, *Macromolecules*, 39 (2006) 4775-4787.
- [24] Puskar, L., E. Ritter, U. Schade, M. Yandrasits, S. J. Hamrock, M. Schaberg, E. F. Aziz, Infrared dynamics study of thermally treated perfluoroimide acid proton exchange membranes. *Phys. Chem. Chem. Phys.* 19 (2017) 626–635.
- [25] B. R. Matos, E. I. Santiago, J. F. Q. Rey, C. H. Scuracchio, G. L. Mantovani, L. A. Hirano, F. C. Fonseca, Dc Proton conductivity at low-frequency in Nafion conductivity spectrum probed by time-resolved SAXS measurements and impedance spectroscopy, *J. Polym. Sci. Part B: Polym. Phys.* 53 (2015) 822.
- [26] V. Felice, S. Ntais, A. C. Tavares, Propyl sulfonic acid functionalization of faujasite-type zeolites: Effect on water and methanol sorption and on proton conductivity, *Microporous and Mesoporous Materials* 169 (2013) 128–136.
- [27] S. A. Perusich, FTIR Equivalent Weight Determination of Perfluorosulfonate Polymers, *J. Appl. Polym. Sci.*, 120 (2011)165–183.
- [28] K. M. Cable, K. A. Mauritz, and R. B. Moore, Effects of Hydrophilic and Hydrophobic Counterions on the Coulombic Interactions in Perfluorosulfonate Ionomers, *Journal of Polymer Science: Part B: Polymer Physics*, 33 (1995) 1065-1072.
- [29] H. Kim, S. Prakash, W. E. Mustain<sup>1</sup>, P. A. Kohl, Sol–gel based sulfonic acid-functionalized silica proton conductive membrane, *J. Power Sources* 193 (2009) 562–569.
- [30] Y. Zhou, R. Huang, F. Ding, A. D. Brittain, J. Liu, M. Zhang, M. Xiao, Y. Meng, L. Sun, Sulfonic Acid-Functionalized  $\alpha$ -Zirconium Phosphate Single-Layer Nanosheets as a Strong Solid Acid for Heterogeneous Catalysis Applications, *ACS Appl. Mater. Interfaces*, 6 (2014) 7417–7425.

[31] K. A. Page, K. M. Cable, R. B. Moore, Molecular origins of the thermal transitions and dynamic mechanical relaxations in perfluorosulfonate ionomers, *Macromolecules* 38 (2005) 6472.

[32] Schönhals, A.; Kremer, F. in *Broadband Dielectric Spectroscopy*. F. Kremer, A. Schönhals, Eds; Springer Verlag, Berlin, 2003, p. 59.

[33] B. R. Matos, J. S. da Silva, E. I. Santiago, D. F. Parra, D. J. Carastan, D. Z. de Florio, H. E. Andrada, A. C. Carreras, F. C. Fonseca, Proton and cesium conductivity in perfluorosulfonate ionomers at low and high relative humidity. *Solid State Ionics* 301 (2017) 86–94.